Monthly Notices
of the
ROYAL ASTRONOMICAL SOCIETY

Mon. Not. R. Astron. Soc. **419,** 2783–2796 (2012) doi:10.1111/j.1365-2966.2011.19921.x

Measuring expansion velocities in Type II-P supernovae

K. Takáts[1⋆] and J. Vinkó[1,2⋆]

[1]*Department of Optics and Quantum Electronics, University of Szeged, Dóm tér 9, Szeged, Hungary*
[2]*Department of Astronomy, University of Texas at Austin, Austin, TX 78712, USA*

Accepted 2011 September 28. Received 2011 September 28; in original form 2011 March 28

ABSTRACT

We estimate photospheric velocities of Type II-P supernovae (SNe) using model spectra created with SYNOW, and compare the results with those obtained either by more conventional techniques, such as cross-correlation, or by measuring the absorption minimum of P Cygni features. Based on a sample of 81 observed spectra of five SNe, we show that SYNOW provides velocities that are similar to those obtained by more sophisticated non-local thermodynamic equilibrium modelling codes, but they can be derived in a less computation-intensive way. The estimated photospheric velocities ($v_{\rm model}$) are compared to those measured from Doppler shifts of the absorption minima of the Hβ and the Fe II λ5169 features.

Our results confirm that Fe II velocities ($v_{\rm Fe}$) have a tighter and more homogeneous correlation with the estimated photospheric velocities than those measured from Hβ, but both suffer from phase-dependent systematic deviations. The same is true for a comparison with the cross-correlation velocities. We verify and improve the relations between $v_{\rm Fe}$, $v_{\rm H\beta}$ and $v_{\rm model}$ in order to provide useful formulae for interpolating/extrapolating the velocity curves of Type II-P SNe to phases not covered by observations. We also discuss implications of our results for the distance measurements of Type II-P SNe and show that the application of the model velocities is preferred in the expanding photosphere method.

Key words: supernovae: general – supernovae: individual: SN 1999em – supernovae: individual: SN 2004dj – supernovae: individual: SN 2004et – supernovae: individual: SN 2005cs – supernovae: individual: SN 2006bp.

1 INTRODUCTION

Type II-P supernovae (SNe) are core-collapse (CC) induced explosions that eject massive hydrogen-rich envelopes. These SNe show a nearly constant-luminosity plateau in their light curve. The plateau phase lasts for ∼100 d, and finally ends up in a rapid decline of the luminosity as the expanding ejecta become fully transparent.

CC SNe and their progenitors play important role in understanding the evolution of the most massive stars. Extensive searches for SN progenitors showed that the progenitors of Type II-P SNe are stars with initial masses between ∼8 and 17 $M_\odot$ (Smartt et al. 2009). The lower value is roughly in agreement with the prediction of current theoretical evolutionary tracks, but the upper limit is somewhat lower than expected. The fate of the more massive ($M \geq 20\ M_\odot$) stars is controversial. They are thought to be the input channel for Type Ib/c SNe (Gaskell et al. 1986), but this has not been confirmed directly by observations yet (Smartt 2009).

Any observational study of the physics of SNe and their progenitors (and, obviously, all astronomical objects) depends heavily on the knowledge of their distances. Because distance is such a crucial parameter, strong efforts have been devoted to the development of distance measurement techniques that are applicable for Type II-P SNe.

The expanding photosphere method (EPM) (Kirshner & Kwan 1974), a variant of the Baade–Wesselink method, uses the idea of comparing the angular and the physical diameter of the expanding SN ejecta. The input quantities are fluxes, temperatures and velocities observed at several epochs during the photospheric phase. Thus, EPM requires both photometric and spectroscopic monitoring of SNe throughout the plateau phase. A clear advantage of EPM is that it does not require external calibration via SNe with known distances. Another interesting property is that EPM is much less sensitive to uncertainties in the interstellar reddening and absorption towards SNe. As Eastman, Schmidt & Kirshner (1996, hereafter E96) have shown, 1-mag uncertainty in A_V results in only ∼8 per cent error in the derived distance. However, the assumption that the SN atmosphere radiates as a blackbody diluted by electron scattering has raised some concerns. These led to the development of the applications of full non-local thermodynamic equilibrium (NLTE) model atmospheres, such as the PHOENIX code in the spectral-fitting expanding atmosphere method (SEAM; Baron et al. 2004) or the CMFGEN code by Dessart & Hillier (2005a,b). The drawback of these

⋆E-mail: ktakats@titan.physx.u-szeged.hu (KT); vinko@titan.physx.u-szeged.hu (JV)

Table 1. Physical properties of the supernovae used in this paper.

SN	t_0 (JD 245 0000)	Distance (Mpc)	cz^a (km s^{-1})	$E(B-V)$ (mag)	$M_{\rm Ni}$ (10^{-2} M$_\odot$)	$M_{\rm prog}$ (M$_\odot$)	References[b]
SN 1999em	1477.0	7.5–12.5	717	0.10	2.2 – 3.6	<15	1, 2, 3, 4, 5, 6, 7, 8
SN 2004dj	3187.0	3.2–3.6	131	0.07	1.3–2.2	12–20	9, 10, 11, 12, 13, 14, 15
SN 2004et	3270.5	4.7–6.0	48	0.41	5.6–6.8	9, 15–20	16, 17, 18, 19, 20, 21, 22
SN 2005cs	3549.0	7.1–8.9	463	0.05	0.3–0.8	6–13	23, 24, 25, 26, 27, 28, 29
SN 2006bp	3835.1	17.0–18.3	987	0.40	–	12–15	26, 30

[a]NED, http://nedwww.ipac.caltech.edu/

[b] *References*: (1) Hamuy et al. (2001); (2) Leonard et al. (2002); (3) Smartt et al. (2002); (4) Leonard et al. (2003); (5) Elmhamdi et al. (2003); (6) Baron et al. (2004); (7) Dessart & Hillier (2006); (8) Utrobin (2007); (9) Maíz-Apellániz et al. (2004); (10) Kotak et al. (2005); (11) Wang et al. (2005); (12) Chugai et al. (2005); (13) Zhang et al. (2006); (14) Vinkó et al. (2006); (15) Vinkó et al. (2009); (16) Li et al. (2005); (17) Sahu et al. (2006); (18) Misra et al. (2007); (19) Utrobin & Chugai (2009); (20) Poznanski et al. (2009); (21) Maguire et al. (2010b); (22) Crockett et al. (2011); (23) Maund, Smartt & Danziger (2005); (24) Pastorello et al. (2006); (25) Takáts & Vinkó (2006); (26) Dessart et al. (2008); (27) Eldridge, Mattila & Smartt (2007); (28) Utrobin & Chugai (2008); (29) Pastorello et al. (2009); (30) Immler et al. (2007).

approaches is that the building of tailored model atmospheres can be very time-consuming and needs much more computing power. Also, in order to compute reliable models, the input observed spectra need to have sufficiently high signal-to-noise ratio (S/N) and spectral resolution.

The more recently developed standardized candle method (SCM; Hamuy & Pinto 2002; Hamuy 2003) relies on the empirical correlation between the measured expansion velocity and the luminosity either in optical (Nugent et al. 2006; Poznanski et al. 2009) or in near-infrared (Maguire et al. 2010a) bands in the middle of the plateau phase, at +50 d after explosion. This method requires less extensive input data, but needs a larger sample of Type II SNe with independently known distances in order to calibrate the empirical correlation. Because this is basically a photometric method which compares apparent and absolute magnitudes, SCM is more sensitive to interstellar reddening than EPM/SEAM, as mentioned above.

Besides photometry, both EPM/SEAM and SCM need information on the expansion velocity at the photosphere ($v_{\rm phot}$). At first, EPM seems to be more challenging, because it requires multi-epoch observations, while SCM needs only the velocity at a certain epoch, at +50 d after explosion (v_{50}). However, direct measurement of v_{50} is possible only in the case of precise timing of the spectroscopic observation, which is rarely achievable.

The correct determination of $v_{\rm phot}$ is not trivial. As SNe expand homologously ($v \sim r$, where v is the velocity of a given layer and r is its distance from the centre), in most cases it is difficult to derive a unique velocity from the observed spectral features. The most frequently followed approach relies on measuring the Doppler shift of the absorption minimum of certain spectral features (mostly Fe II λ5169 or Hβ). Another possibility is the computation of the cross-correlation between the SN spectrum and a set of spectral templates, consisting of either observed or model spectra, with known velocities. The third method is building a full NLTE model (such as PHOENIX or CMFGEN) for a given SN spectrum and adopting the theoretical $v_{\rm phot}$ from the best-fitting model.

The aim of this paper is to present a similar, but less computation-demanding approach to assign velocities to observed SN spectra. We apply the simple parametrized code SYNOW (Fisher 1999; Hatano et al. 1999) to model the observed spectra with an approximate, but self-consistent treatment of the formation of lines in the extended, homologously expanding SN atmosphere. To illustrate the applicability of SYNOW, we construct and fitted parametrized models to a sample of five well-observed, nearby Type II-P SNe that have a series of high-S/N spectra publicly available. We also check and re-calibrate some empirical correlations between velocities derived from various methods. The description of the observational sample is given in Section 2. In Section 3 we first review the different velocity measurement techniques for SNe II-P, and then we present the details of the application of SYNOW models (Section 3.4). The results are collected and discussed in Sections 4 and 5, while the implications of the results for the distance measurements are given in Section 6. We draw our conclusions in Section 7.

2 DATA

Our sample contains 81 plateau phase spectra of five objects, SNe 1999em, 2004dj, 2004et, 2005cs and 2006bp. All five SNe are well-observed objects, they have been studied in detail and show a wide variety in their physical properties (see Table 1).

SN 1999em was discovered on 1999 October 29 by Li (1999) in NGC 1637 at a very early phase. It is a very well-observed, well-studied object. The explosion date was determined as 245 1477.0 ± 2 JD (Hamuy et al. 2001; Leonard et al. 2002; Dessart & Hillier 2006). We used the spectra of Leonard et al. (2002) and Hamuy et al. (2001) downloaded from the SUSPECT[1] data base. Our sample contains 22 spectra, covering the first 80 d of the plateau phase.

SN 2004dj was discovered on 2004 July 31 by Itagaki (Nakano et al. 2004) in a young, massive cluster Sandage-96 of NGC 2403, about 1 month after explosion. We used the spectra taken by Vinkó et al. (2006). Due to the lack of observed spectrophotometric standards, the flux calibration of those spectra was inferior, but this is not a major concern when only velocities are to be determined. We included 12 spectra taken between +47 and +100 d after explosion in our sample.

SN 2004et was discovered by Moretti (Zwitter, Murani & Moretti 2004) on 2004 September 27 in NGC 6946. The spectra of Sahu et al. (2006) (downloaded from SUSPECT) and Maguire et al. (2010b) were used, together with six previously unpublished early-phase spectra taken with the 1.88-m telescope at the David Dunlap Observatory (DDO; see Appendix A). The 22 spectra cover the period of +11 to +104 d after explosion.

SN 2005cs was discovered on 2005 June 29 by Kloehr et al. (2005) in M51. Due to its very early discovery and proximity, this object is very well sampled and studied in detail. It is an underluminous, low-energy, Ni-poor SN that had a low-mass progenitor (see

[1] Available from http://suspect.nhn.ou.edu/~suspect/

Table 1 for references). 14 spectra of Pastorello et al. (2006, 2009) were used, which were obtained between days +3 and +61.

SN 2006bp was discovered on 9th April 2006 by Nakano & Itagaki (2006) in NGC 3953, also in a very early phase. We used 11 spectra of Quimby et al. (2007), downloaded from SUSPECT, covering the period between +5 and +72 d.

3 THE ISSUE OF MEASURING EXPANSION VELOCITIES IN SNe

During the photospheric phase, the homologously expanding Type II-P SN ejecta consist of two parts: the outer, partly transparent atmosphere where the observable spectral features are formed, and an optically thick inner part, which emits most of the continuum radiation as a 'diluted' blackbody (e.g. E96). Because the inner part is mostly ionized, the major source of the total opacity is electron scattering. Thus, the *instantaneous* photosphere is located at the depth where the outgoing photons are last scattered, i.e. where the electron-scattering optical depth is $\tau_e \sim 2/3$ (Dessart & Hillier 2005a, hereafter D05). This is presumed to occur in a thin, spherical shell at a certain radius $r_{\rm phot}$, and the homologous expansion gives this a unique velocity $v_{\rm phot} = v_{\rm ref}\, r_{\rm phot}/r_{\rm ref}$, where $r_{\rm ref}$ is the radius of an (arbitrary) reference layer and $v_{\rm ref}$ is its expansion velocity. As the ejecta expand and dilute, the photosphere migrates inwards, towards the inner layers of the ejecta that expand at a slower rate; thus $v_{\rm phot}$ continuously declines with time.

The issue of measuring $v_{\rm phot}$ comes from the fact that no measurable spectral feature is connected directly to $v_{\rm phot}$. As previously mentioned in Section 1, there exist several observational/theoretical approaches to *estimate* $v_{\rm phot}$ from observed spectra. In the following, we briefly review these methods, summarizing their advantages/drawbacks.

3.1 P Cygni lines

The most widely used method is to measure the velocity represented by the minimum flux of the absorption component of an unblended P Cygni line profile (sometimes referred to as 'maximum absorption', $v_{\rm abs}$; Dessart & Hillier 2005b). This is motivated by the theory of P Cygni line formation (e.g. Kasen et al. 2002), which predicts that the minimum flux in a P Cygni line occurs at the velocity of the photosphere. Strictly speaking, this is only true for an optically thin line formed by pure scattering. In most cases, the Fe II λ5169 feature is used for measuring $v_{\rm abs}$, for which Dessart & Hillier (2005b) pointed out that it can represent the true $v_{\rm phot}$ within 5–10 per cent accuracy. However, Leonard et al. (2002) showed that using weaker, unblended features one can get ∼10 per cent lower velocities than from the Fe II λ5169 feature. This raises the question of whether the measurable lines were indeed optically thin and unblended, and which one represented the true $v_{\rm phot}$. Moreover, Dessart & Hillier (2005b) also revealed that $v_{\rm abs}$ can either overestimate or underestimate $v_{\rm phot}$, depending on various physical conditions, such as the density gradient and the excitation/ionization conditions for the particular transition within the ejecta.

While the Fe II λ5169 feature can be relatively easily identified and measured in Type II-P SNe spectra obtained later than ∼20 d after explosion (which is undoubtedly a major advantage of this method), this is not so for earlier phases. In early-phase spectra only the Balmer lines and maybe He I features (mostly the λ5876 feature) can be identified. These features are less useful for measuring $v_{\rm phot}$, because none of them is optically thin and the He I λ5876 feature can sometimes be blended with Na I D. Moreover, their line profile shapes often make the location of the minimum of absorption component difficult to determine (Dessart & Hillier 2005b, 2006).

Also, in spectra having less S/N, the weaker Fe II features are often buried in the noise, making them inappropriate for velocity measurement. In these cases, several authors attempted to use the stronger features, especially Hβ. Although Dessart & Hillier (2005b) pointed out that $v_{\rm H\beta}$ is certainly less tightly connected to $v_{\rm phot}$ than the weaker Fe II λ5169 feature, Nugent et al. (2006) have shown that the ratio $v_{\rm H\beta}/v_{\rm Fe}$ is ∼1.4 below $v_{\rm H\beta} = 6000\,{\rm km\,s^{-1}}$ and linearly decreases for higher velocities. Recently, this correlation was revised by Poznanski, Nugent & Filippenko (2010) by revealing an entirely linear relation between $v_{\rm H\beta}$ and $v_{\rm Fe}$, but restricting the analysis only to velocities measured between +5 and +40 d after explosion. The uncertainty of estimating $v_{\rm Fe}$ from $v_{\rm H\beta}$ is $\sim 300\,{\rm km\,s^{-1}}$ (Poznanski et al. 2010). It is emphasized that these empirical relations are more or less valid between the velocities of two observable features, but both of them may be systematically off from the true $v_{\rm phot}$. Indeed, Dessart & Hillier (2005b) found that $v_{\rm H\beta}$ can be either higher or lower than $v_{\rm phot}$ with an overall scattering of ±15 per cent. For velocities below $10\,000\,{\rm km\,s^{-1}}$ $v_{\rm H\beta}$ is usually higher than $v_{\rm phot}$, in accord with the empirical correlations with $v_{\rm Fe}$, but above $10\,000\,{\rm km\,s^{-1}}$ it can be lower than $v_{\rm phot}$.

3.2 Cross-correlation

Motivated by the uncertainties of measuring the Doppler shift of a single, weak feature in a noisy spectrum, several authors proposed the usage of the cross-correlation technique, which is a powerful method for measuring Doppler shifts of stellar spectra containing many narrow spectral features. This method predicts the Doppler shift of the *entire* spectrum by computing the cross-correlation function (CCF) between the observed spectrum and a template spectrum with a priori known velocity $v_{\rm templ}$. The resulting velocity is $v_{\rm cc} = v_{\rm rel} + v_{\rm templ}$, where $v_{\rm rel}$ is the velocity at which the CCF reaches its maximum (i.e. the relative Doppler shift between the observed spectrum and the template).

However, the applicability of cross-correlation for SN spectra is not obvious, because of the physics of P Cygni line formation in SN atmospheres. If $v_{\rm phot}$ is higher, then the centre of the absorption component gets blueshifted, while the centre of the emission component stays close to zero velocity. Thus, cross-correlating two spectra with different $v_{\rm phot}$, the relative velocity will underestimate the true velocity difference between the two spectra. This is illustrated in Fig. 1, where we determined the CCF between two Type II-P SN model spectra (computed with SYNOW, see below) that were identical except their $v_{\rm phot}$ which differed by $\Delta v_{\rm phot} = 2000\,{\rm km\,s^{-1}}$. The cross-correlation was computed only in the 4500–5500 Å interval to exclude the Hα feature. This was done for an early-phase spectrum containing only H and He features (Fig. 1, left panel) and a later-phase spectrum with more developed metallic lines (Fig. 1, right panel). It is visible in the bottom panels that the maximum of the CCF (i.e. $v_{\rm rel}$) is shifted towards lower velocities with respect to the true $\Delta v_{\rm phot}$ (indicated by a dotted vertical line in the CCF plot) for both spectra. The systematic offset of $v_{\rm rel}$ from $\Delta v_{\rm phot}$ is $\sim 200\,{\rm km\,s^{-1}}$ for the later-phase spectrum that contains many narrower absorption features, and it reaches $\sim 700\,{\rm km\,s^{-1}}$ for the early-phase spectrum that is dominated by broad Balmer lines with a stronger emission component. These simple tests are in very good agreement with the results of Hamuy et al. (2001) and Hamuy (2002), who applied the cross-correlation technique using model spectra of E96 with a-priori known $v_{\rm phot}$ as templates.

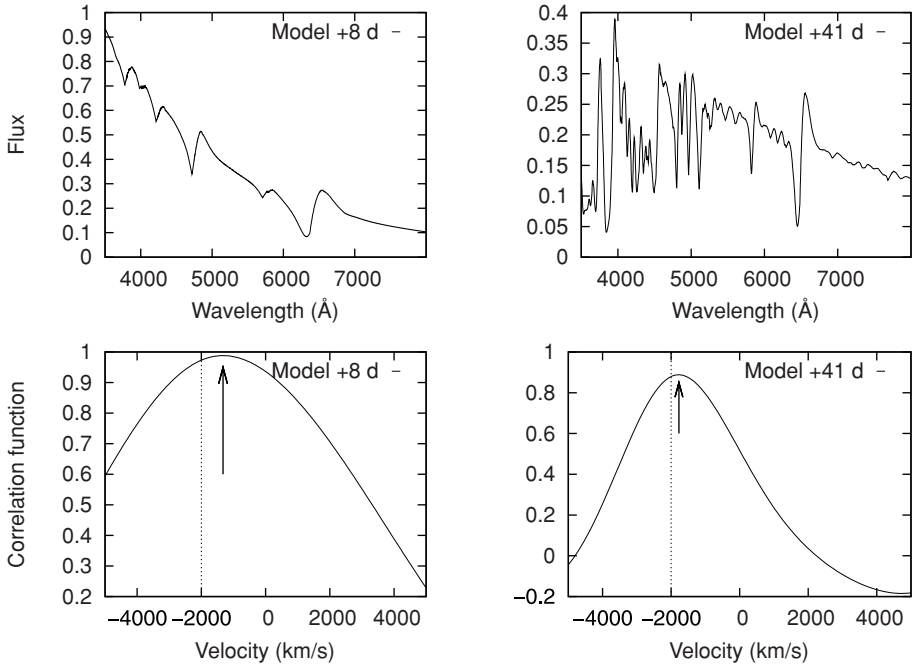

Figure 1. Model spectra of a Type II-P SN in the early-phase (top left) and late-phase (top right), and the resulting CCFs (bottom panels) after cross-correlating the spectra with their identical models but having a 2000 km s^{-1} higher $v_{\rm phot}$. The arrows mark the peak location of the CCFs, while the true relative velocity difference $\Delta v_{\rm phot}$ is indicated by the dotted vertical line. The peak of the CCF underestimates $\Delta v_{\rm phot}$ in both cases.

They pointed out that $v_{\rm rel}$ usually underestimates $\Delta v_{\rm phot}$ so that $\Delta v_{\rm phot}/v_{\rm rel} \sim 1.18$, with the scatter of $\sim$900 km s^{-1}.

Another variant of the CCF method was proposed by Poznanski et al. (2009), and was also applied by D'Andrea et al. (2010) and Poznanski et al. (2010). They took their template spectra from the library of the SuperNova IDentification code SNID[2] (Blondin & Tonry 2007) that contains high-S/N observed spectra of many SNe, but used only those templates that showed a well-developed Fe II λ5169 feature. The reason for their choice was that they wanted to estimate $v_{\rm Fe}$ at +50 d after explosion (v_{50}), which is an input parameter in SCM. This template selection caused the well-known issue of template mismatch that further biases the cross-correlation results. As D'Andrea et al. (2010) concluded, this template mismatch can result in significant underestimate of $v_{\rm Fe}$ by $\sim$1500 km s^{-1} for spectra obtained at $t < 20$ d, and is also present in later-phase spectra, although it is less pronounced, $\sim$300–400 km s^{-1}. To overcome this problem, in a subsequent paper Poznanski et al. (2010) suggested the application of their $v_{\rm Fe}$ versus $v_{\rm H\beta}$ relation to estimate $v_{\rm Fe}$ by measuring $v_{\rm H\beta}$ for these early-phase spectra and then propagate the resulting velocity to day +50. Nevertheless, the two groups presented velocities that were different by 200 to 1000 km s^{-1} for the same set of SNe spectra from the Sloan Digitized Sky Survey-II (SDSS-II). This underlines that although cross-correlation seems to be an easy and robust method that gives reasonable velocities even for low-S/N spectra, the results may be heavily biased, especially at early phases, when the SN spectra contain only a few, broad features.

3.3 Tailored modelling

Tailored modelling of the whole observed spectrum via NLTE models was invoked e.g. by Baron et al. (2004) using the code PHOENIX, and Dessart & Hillier (2006) and Dessart et al. (2008) with the code CMFGEN. Here, $v_{\rm phot}$ is determined implicitly by requiring an overall fit of the entire observed spectrum by a synthetic spectrum from a full NLTE radiation-hydrodynamic model. In these models the location of the photosphere is usually defined as the layer where the electron scattering optical depth reaches unity or 2/3 (e.g. D05). $v_{\rm phot}$ is then simply determined by the radius $r_{\rm phot}$ and the law of homologous expansion (see above). Although this is probably the best self-consistent method for obtaining SN velocities, building full NLTE models for multiple epochs requires a large amount of computing power. Thus, its usage for a larger sample of SNe would be very time-consuming and impractical. Also, in some cases a good global fit to the whole spectrum may not be equally good for individual spectral lines, where a large number of physical details play important role in the formation of the given features. This may lead to some uncertainties in the velocities given by the models, which will be illustrated in Section 4.

3.4 Using SYNOW

The success of tailored spectrum models to estimate $v_{\rm phot}$ suggests a similar, but much more simplified approach: the usage of *parametrized* spectrum models that do not contain the computation-intensive details of NLTE level populations or exact radiative transfer calculations, but preserve the basic physical assumptions of an expanding SN atmosphere, and able to reproduce the formation of P Cygni lines in a simplified manner. Such models can be computed either with the SYNOW code (Branch et al. 2002) or using the more recently developed SYNAPPS code (Thomas, Nugent & Meza 2011) that has a parameter-optimizer routine built-in. In this paper we apply SYNOW to calculate model spectra. Because SYNOW does only spectrum synthesis and has no fitting capabilities, we used self-developed UNIX shell scripts to fine-tune the parameters until a satisfactory fit to the observed spectrum is achieved.

[2] Available from http://marwww.in2p3.fr/~blondin/software/snid/index.html

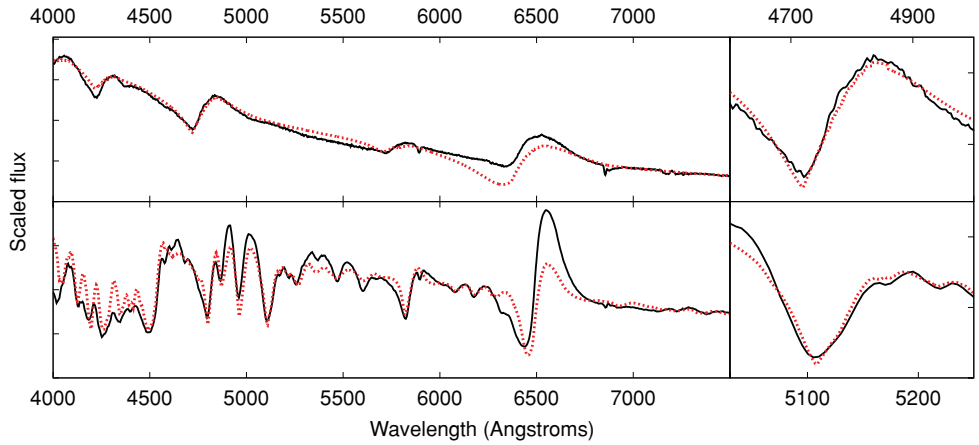

Figure 2. The observed (black solid line) and best-fitting model (red dashed line) spectra of SN 1999em on days +9 (top) and +41 (bottom). The right panels enlarge the wavelength regions of the fitted lines: Hβ (top) and Fe II λ5169 (bottom).

The basic assumptions of SYNOW are the followings: (i) the SN ejecta expand homologously; (ii) the photosphere radiates as a blackbody; (iii) spectral lines are formed entirely above the photosphere; (iv) the line formation is due to pure resonant scattering. Level populations are treated in LTE and the radiative transfer equation is solved in the Sobolev approximation (see also e.g. Kasen et al. 2002).

When running SYNOW, several parameters must be set. These are the temperature of the blackbody radiation ($T_{\rm bb}$) emitted by the photosphere, the expansion velocity at the photosphere ($v_{\rm phot}$), the chemical composition of the ejecta and the optical depth of a reference line ($\tau_{\rm ref}$) of each compound. For each atom/ion, the optical depths for the rest of the lines are calculated assuming Boltzmann excitation governed by the excitation temperature $T_{\rm exc}$. The location of the line-forming region in the atmosphere can be tuned for each compound by setting the velocities of the lower and upper boundary layers, $v_{\rm min}$ and $v_{\rm max}$. The optical depth as a function of velocity (i.e. radius) can be modelled either as a power law or as an exponential function. We assumed power-law atmospheres and adjusted the power-law exponent n to reach optimal fitting.

After setting the initial values by hand, several models in a wide range of $v_{\rm phot}$, n and $\tau_{\rm ref}$ were created for a pre-selected set of ions. In order to reduce the number of free parameters, we initially set $T_{\rm bb}$ (which has very little effect on the line shapes) to represent the continuum of the fitted spectrum and kept it fixed during the optimization. Moreover, we applied a single power-law exponent n for all atoms/ions. We also assumed that all spectral features are photospheric, thus fixing $v_{\rm min}$ well below the photosphere and $v_{\rm max}$ at $\sim$40 000 km s^{-1}.

The best-fitting model was then chosen via χ^2-minimization, and the fitting process was iterated for a few times, each time resampling the parameter grid in the vicinity of the minimum of the χ^2 function found in the previous iteration cycle. This way we determined the parameters and the chemical compositions that best describe the observed spectra.

Then, to further refine the estimated photospheric velocity, we fine-tuned only $v_{\rm phot}$ of the best-fitting model and calculated the χ^2 function only in the vicinity of certain lines instead of the whole spectrum. This may reduce the systematic underestimate or overestimate of $v_{\rm phot}$ produced by false positive fitting to the observed spectrum outside the range of the spectral features considered.

Motivated by the results of Dessart & Hillier (2005b) (see Section 3.1), we have chosen the Fe II λ5169 feature for this fine-tuning process. When this feature was not present in the observed spectrum (i.e. the early-phase spectra, before $\sim$15 d), we used Hβ (see Section 3.1) instead. Hereafter we denote the $v_{\rm phot}$ parameter of the best-fitting SYNOW model as $v_{\rm model}$. Errors of $v_{\rm model}$ were estimated by choosing the 90 per cent confidence interval around the minimum of the χ^2 function.

Fig. 2 shows two examples for an early- and a later-phase spectrum of SN 1999em together with the best-fitting model. The right-hand panel zooms in on the region of Hβ and Fe II λ5169. Note that although the final fitting was restricted to the proximity of these lines, the best model describes the entire observed spectrum (except Hα) very well.

This velocity measurement method has multiple sources of error. One of them may be the systematic bias due to the approximations in the model (LTE, power-law atmosphere, simple source function etc.). However, the comparison of our results with those from full NLTE CMFGEN models (Section 4) shows no systematic bias in the case of SNe 1999em and 2005cs. The agreement between the velocities from these two very different modelling codes is within $\pm$10 per cent. For SN 2006bp, the differences are higher, but it will be shown below that for this SN the CMFGEN models do not describe well the spectral features we use, in contrast to the SYNOW models (Section 4.5).

Another source of error may be the correlation between the parameters. In Fig. 3 we present contour plots of the χ^2 hyperspace around its minimum, as a function of $v_{\rm model}$ and several other parameters that can affect the shape of the fitted Fe II λ5169 feature. The thick black contour curve corresponds to 50 per cent higher χ^2 than the minimum value. It is visible that the correlation is indeed present (i.e. the contours are distorted) between $v_{\rm model}$ and the power-law exponent n or the optical depth $\tau_{\rm Fe}$. The correlation is much less between $v_{\rm model}$ and $\tau_{\rm ref}$ of Ti II and Mg I, whose features may blend with Fe II λ5169. However, even for the correlated parameters, selecting n or $\tau_{\rm Fe}$ very far from their optimum value can alter $v_{\rm model}$ only by a few hundred km s^{-1}. Thus, we conclude that uncertainties in finding the minimum of χ^2 do not cause errors in $v_{\rm model}$ that significantly exceed the uncertainty due to the spectral resolution of the observed spectra (which is usually between 200 and 300 km s^{-1}).

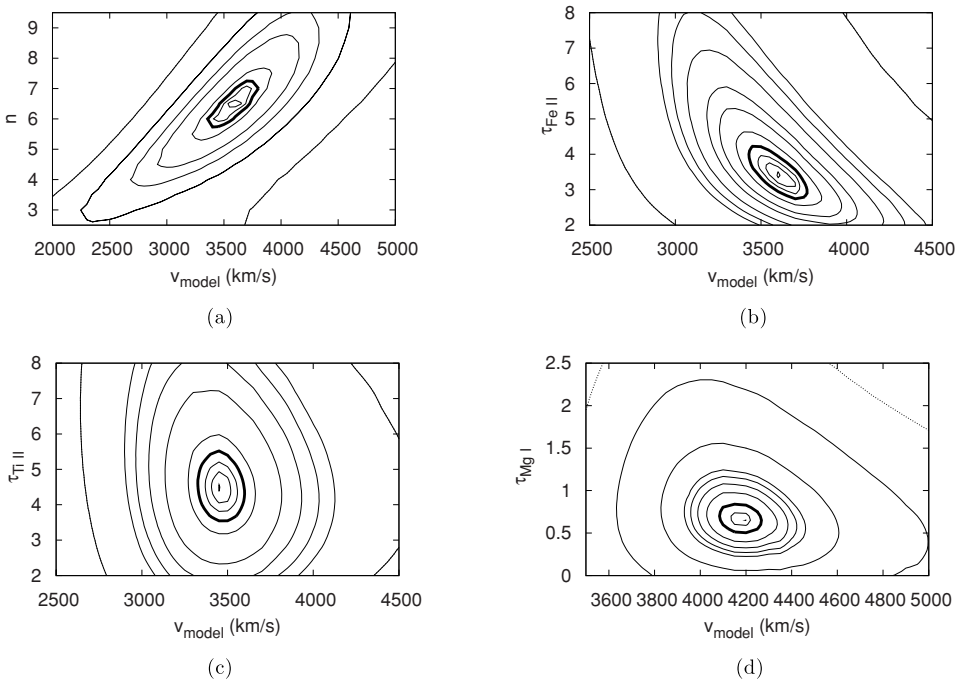

Figure 3. Contour plot of the χ^2 function around its minimum, as a function of $v_{\rm model}$ and power-law exponent n (a), $\tau_{\rm ref}$ of Fe II (b), Ti II (c) and Mg I (d). The thick black contour curve corresponds to 50 per cent higher χ^2 than the minimum value. The parameters plotted in (a) and (b) are definitely correlated, while the correlation is much less between the parameters in (c) and (d).

A possible source of uncertainty may be that during the final fitting the wavelength interval around the used spectral feature is chosen somewhat subjectively. However, our tests showed that changing the limits reasonably has a negligible effect on the final velocities.

It is emphasized that although the final fitting is restricted to the vicinity of a well-defined spectral line, this method is certainly more reliable than the measurement of only the location of the *minimum* of the same feature. As discussed above, the minimum can be significantly and systematically altered by S/N, spectral resolution, blending etc. The fitting of a model spectrum to the *entire* feature is expected to overcome these difficulties, provided the underlying model is not too far from reality.

4 COMPARING THE RESULTS FROM DIFFERENT METHODS

Using SYNOW as described above, we determined the best-fitting parameters of all SNe spectra from Section 2. The resulting model velocities are collected in Table B1 in Appendix B. The best-fitting SYNOW parameters, such as $\tau_{\rm ref}$ for each atom/ion, the power-law exponent n and $v_{\rm model}$ together with the chosen $T_{\rm phot}$, can be found in Table C1 in Appendix C. In Table B1 we also list the $v_{\rm Fe}$ and $v_{\rm H\beta}$ velocities. For SNe 1999em, 2005cs and 2006bp, we collected the photospheric velocities from CMFGEN models of Dessart & Hillier (2006) and Dessart et al. (2008). These are included in Table B1 as $v_{\rm nlte}$. Velocities from the cross-correlation technique (Section 3.2) were obtained using two sets of template spectra. The first set contained the 22 observed spectra of SN 1999em (set 1), while the second set was based on the CMFGEN models mentioned above (set 2). The velocities of the template spectra were $v_{\rm Fe}$ for set 1 and $v_{\rm nlte}$ for set 2. We cross-correlated all the observed spectra with the two sets separately on the wavelength range of 4500–5500 Å, and the resulting velocities are also given in Table B1 as $v_{\rm cc}$.

Fig. 4 shows $v_{\rm model}$ against phase for all studied SNe (top left panel) and the ratio of $v_{\rm model}$ to all the other velocities. The calculated velocities all show the expected decline with phase as the photosphere moves much deeper within the ejecta, towards slower expanding layers.

Similar plots containing the ratio $v_{\rm model}/v_{\rm cc}$ and $v_{\rm abs}/v_{\rm cc}$ as functions of phase are presented in Fig. 5.

In the following, we provide some details of deriving these velocities for each object and discuss some object-specific differences between them.

4.1 SN 1999em

When determining $v_{\rm model}$ with SYNOW, Hβ was fitted for the first six spectra, then the Fe II λ5169 feature was used for the remaining 16 spectra. The resulting velocities are between 11 000 and 1800 km s^{-1}. As seen in the bottom right panel of Fig. 4, $v_{\rm model}$ and $v_{\rm H\beta}$ are about the same for the early phases (before the appearance of the Fe II lines), while later $v_{\rm H\beta}$ tends to be higher than $v_{\rm model}$. Also, between day +15 and day +40, $v_{\rm model}$ is slightly higher than $v_{\rm Fe}$ (Fig. 4, bottom left panel). After day +40, $v_{\rm model}$ drops below $v_{\rm Fe}$ and their ratio increases towards later phases.

The velocities from CMFGEN models of Dessart & Hillier (2006) (Fig. 4, top right panel) agree with $v_{\rm model}$. The cross-correlation with set 2 (Fig. 5, bottom panels) gave similar results for the first few points, but overestimate $v_{\rm model}$ between days +22 and +80. They mostly fall between $v_{\rm H\beta}$ and $v_{\rm Fe}$, which is expected, since we cross-correlated the range of 4500–5500 Å, where these features appear.

4.2 SN 2004dj

The SYNOW model velocities of the 11 spectra that cover the second half of the plateau phase are between ∼3400 and 1700 km s^{-1}.

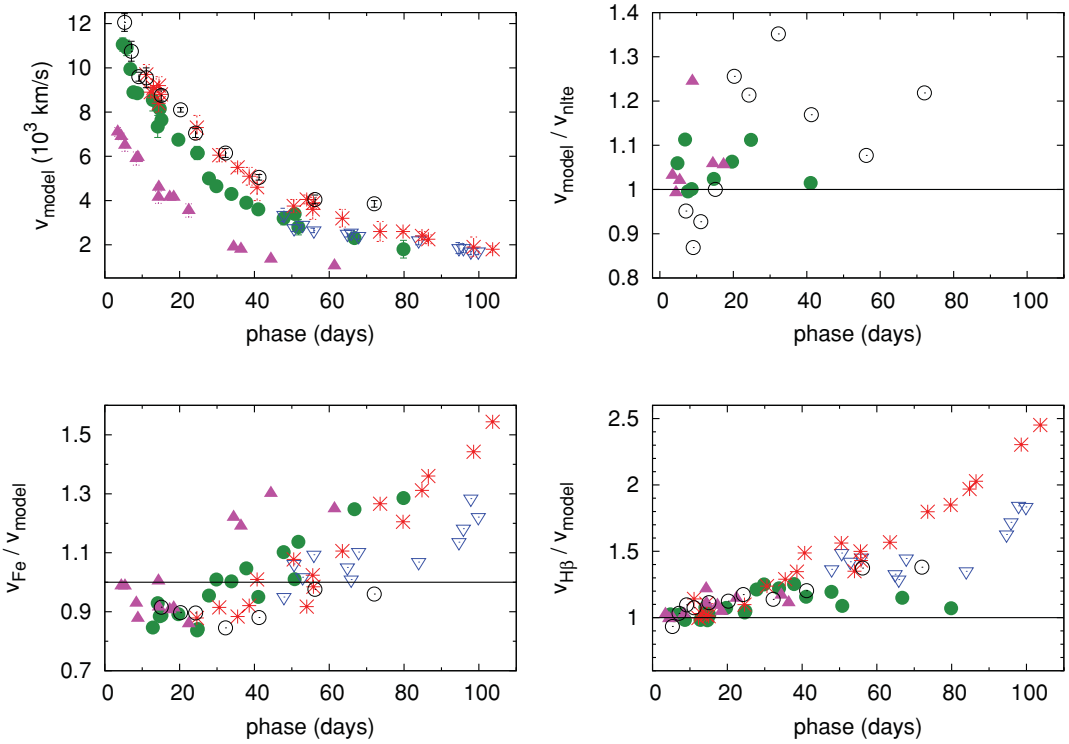

Figure 4. Top left: model velocities ($v_{\rm model}$) from SYNOW as functions of phase. Top right: the ratio of SYNOW and CMFGEN model velocities ($v_{\rm model}/v_{\rm nlte}$) against phase. Bottom panels: the phase dependence of $v_{\rm Fe}/v_{\rm model}$ (bottom left) and $v_{\rm H\beta}/v_{\rm model}$ (bottom right). Symbols represent the following: filled circles, SN 1999em; open circles, SN 2006bp; filled triangles, SN 2005cs; open triangles, SN 2004dj; asterisks, SN 2004et.

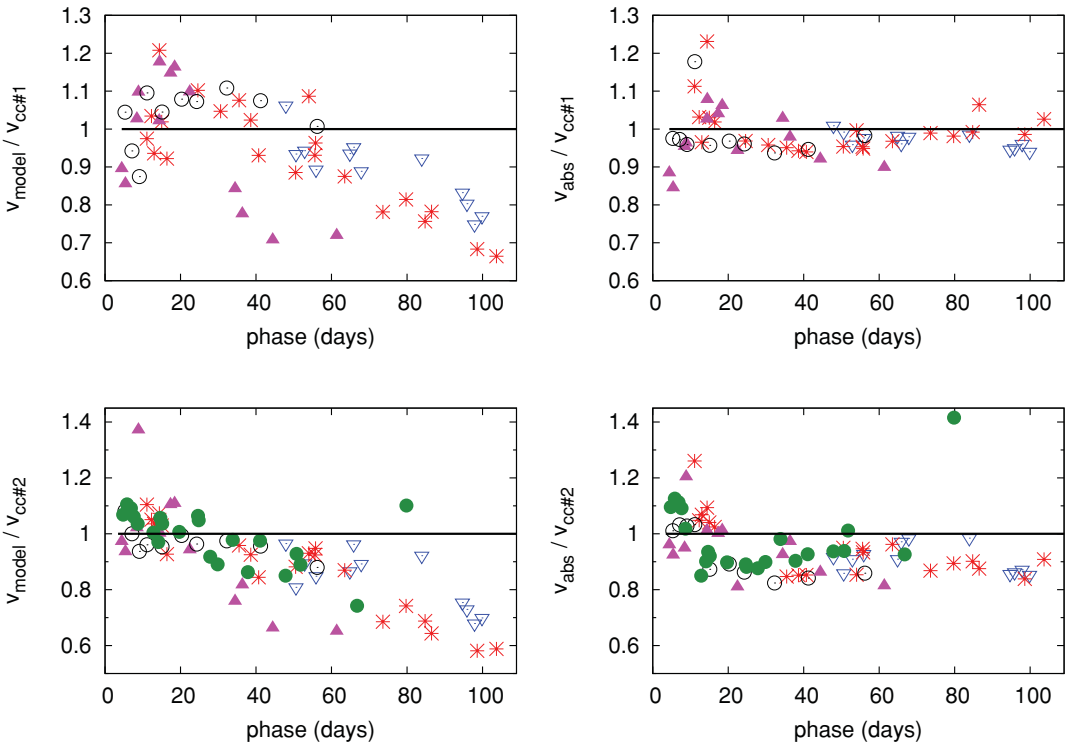

Figure 5. Top panels: ratio of $v_{\rm model}$ and $v_{\rm abs}$ to $v_{\rm cc}$ from cross-correlating with the observed spectra of SN 1999em (set 1, see text) as functions of phase. Bottom panels: the same as above, but with respect to the template set containing CMFGEN models (set 2). The symbols represent the same SNe as in Fig. 4.

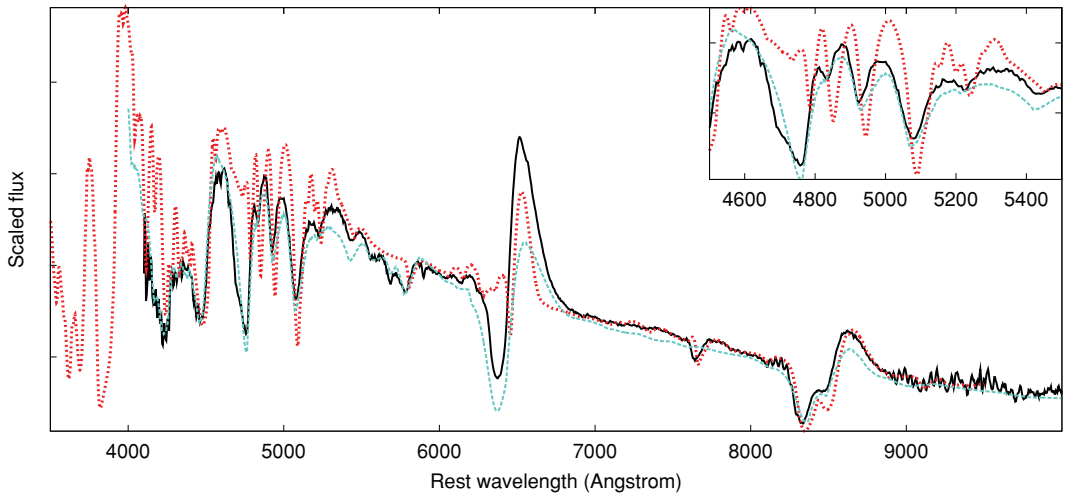

Figure 6. Plot of the CMFGEN (red dotted line) and the SYNOW models (turquoise dashed line) and the observed spectra (black continuous line) of SN 2006bp on day +32 (see text).

These are similar to those of SN 1999em at the same phase. Both $v_{\rm Fe}$ and $v_{\rm H\beta}$ are higher than $v_{\rm model}$ at all epochs, especially the latter with a factor of about 1.8 (Fig. 4).

No CMFGEN model was available for SN 2004dj. Cross-correlation with both template sets gave very similar results. They are only slightly higher than both $v_{\rm model}$ and $v_{\rm Fe}$ (Fig. 5).

4.3 SN 2004et

For the first six spectra, the SYNOW model was optimized for Hβ, then for the Fe II λ5169 feature. The resulting model velocities are between 9700 and 1800 km s^{-1} (Fig. 4). The $v_{\rm Fe}$ values are similar to $v_{\rm model}$, but their ratio shows a slight phase dependence, similar to the other SNe studied here. In contrast, the values of $v_{\rm H\beta}$ are very different from $v_{\rm model}$. At early phases, they are close to $v_{\rm model}$ (except for the first point), but later the $v_{\rm H\beta}$ to $v_{\rm model}$ ratio strongly increases, reaching as high as 2.5.

Again, there is no CMFGEN model available for this SN. Cross-correlation with set 1 resulted in velocities similar to $v_{\rm H\beta}$ at early phases and to $v_{\rm Fe}$ later. With set 2, cross-correlation gave similar results at early phases, but later it produced systematically higher velocities. This underlines the importance of selecting proper template spectra and template velocities when applying the cross-correlation technique.

4.4 SN 2005cs

We used the Hβ line for fitting the first three spectra with SYNOW. The velocities of this SN are very low: they are in the range of 7100–1100 km s^{-1} and decrease quickly. The velocities from absorption minima are very close to $v_{\rm model}$ for both Hβ and Fe II λ5169. The $v_{\rm Fe}$ values follow the tendency similar to the previous objects: they are somewhat lower than $v_{\rm model}$ at the early phases, but become higher after about day +30. The $v_{\rm H\beta}$ values are much closer to $v_{\rm model}$ than for the other SNe, and the $v_{\rm H\beta}/v_{\rm model}$ ratio stays about the same for all epochs (Fig. 4). The velocities of the CMFGEN models for SN 2005cs are the same as the $v_{\rm model}$ values for all epochs, except for day +9. Cross-correlation with both template sets resulted in velocities close to $v_{\rm Fe}$.

4.5 SN 2006bp

The results for SN 2006bp are controversial. Applying SYNOW, the Hβ line was fitted for the first 4 of the 11 observed spectra, while Fe II λ5169 was used for the rest. The model velocities are between 12000 and 3800 km s^{-1}. Both $v_{\rm Fe}$ and $v_{\rm H\beta}$ follow the tendency shown by other SNe (Fig. 4).

In contrast, unlike in the previous two cases, the velocities from the CMFGEN models differ significantly from our $v_{\rm model}$ values. At early epochs, this difference is much lower (∼500–700 km s^{-1}), being close to zero at day +15. After day +15, it becomes higher reaching ∼1200 km s^{-1} on day +32. At later phases, the difference decreases somewhat, but stays being significant.

Cross-correlating the same spectra with the CMFGEN models using the wavelength range of 4500–5500 Å resulted in velocities that are very close to $v_{\rm model}$ (except for day +9). Using the first template set, the results agree well with $v_{\rm Fe}$, or $v_{\rm H\beta}$ at early epochs.

To examine the obvious controversy between the velocity of the CMFGEN models and that of all the others, we plotted the observed spectra and the best-fitting CMFGEN model on day +32 (when the differences are the highest) in Fig. 6. Zooming in on the range of 4500–5500 Å clearly shows that the model by Dessart et al. (2008) does not fit these spectral features well, leading to an underestimate of the velocity. Thus, we suspect that the velocity differences we found are probably due to the inferior fitting of the CMFGEN models to the SN 2006bp spectra.

5 DISCUSSION

As shown in the previous sections, the photospheric velocities of four SNe in our sample evolved similarly. SNe 1999em, 2004et and 2006bp had high velocities at early phases and they decreased quickly, although their decline slopes were different. SN 2004dj probably showed similar evolution, but the lack of the early-phase data prevents a more detailed comparison. In contrast, SN 2005cs was a very different, low-energy SN II-P as discussed in detail in previous studies. It had lower early velocities and the velocity curve decreased much faster than for all the other SNe.

As expected, the different velocity measurement methods we applied provided somewhat different results. As seen in Fig. 5, the velocities obtained from cross-correlation are usually closer to

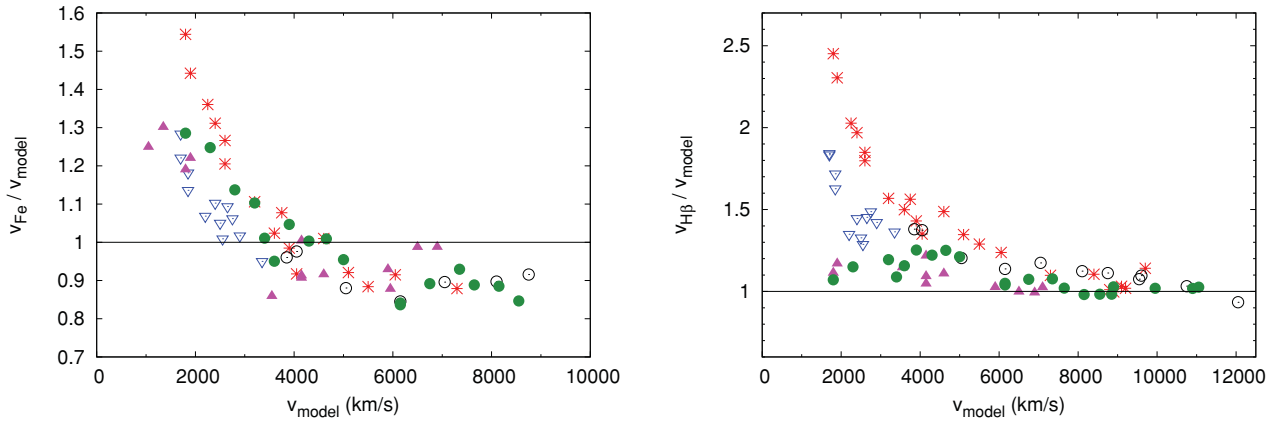

Figure 7. The $v_{\rm Fe}/v_{\rm model}$ (left-hand panel) and $v_{\rm H\beta}/v_{\rm model}$ (right-hand panel) ratio against the model velocities. The symbols have the same meaning as in Fig. 4.

$v_{\rm abs}$ than to $v_{\rm model}$. This is understandable, given that the cross-correlation method is most sensitive to the shapes and positions of the spectral features that may be biased towards lower or higher velocities. The $v_{\rm model}/v_{\rm cc}$ ratio (Fig. 5, top left and bottom left panels) shows the same trend (but plotted upside down) as the $v_{\rm Fe}/v_{\rm model}$ ratio in Fig. 4 (bottom left panel), i.e. $v_{\rm model}$ is higher between days 10 and 50, but becoming smaller than $v_{\rm Fe}$ or $v_{\rm cc}$. On the other hand, no such systematic trend can be identified between $v_{\rm model}$ and $v_{\rm nlte}$ (Fig. 4, top right panel). These benchmarks suggest that the model velocities, either from SYNOW or from CMFGEN, are consistent, and show phase-dependent offsets from the absorption minima or cross-correlation velocities. The increasing systematic offset is particularly strong for $v_{\rm H\beta}$ (Fig. 4, bottom right panel). Thus, the traditional, simple measurement methods seem to underestimate the true photospheric velocities before day 50, but increasingly overestimate them towards later epochs. This should be kept in mind when the true photospheric velocities are needed, e.g. in the application of EPM.

In order to do further testing, we plotted the ratio of $v_{\rm Fe}/v_{\rm model}$ and $v_{\rm H\beta}/v_{\rm model}$ as a function of $v_{\rm model}$ for all SNe, following Dessart & Hillier (2005b) (Fig. 7). The $v_{\rm Fe}/v_{\rm model}$ ratio shows the same trend for all objects: at high velocities (i.e. early phases) the ratio is somewhat lower than 1, then it reaches unity around $\sim$4000 km s^{-1}, and below that it keeps rising, reaching $\sim$ 1.6 by the end of the plateau. The $v_{\rm H\beta}/v_{\rm model}$ ratio is more complicated. At high $v_{\rm model}$ values, it is around 1, but becomes higher than unity around $v_{\rm model} \approx$ 7000 km s^{-1}. Below that the slope of the rising changes from object to object. In the case of SNe 2005cs and 1999em, this ratio stays under $\sim$1.4, while for the other three SNe it becomes much higher. For SN 2006bp, there are no spectra below $v_{\rm model} = 3850$ km s^{-1}, but above that its evolution seems to be similar to that of SN 2004et.

A similar plot was published by Dessart & Hillier (2005b) based on their set of CMFGEN model spectra (see their fig. 14). The only slight difference is that they plotted the ratio of the velocity measured from the absorption minima of the model spectra to the input velocity of the code, as a function of the input velocities. Although they did not have data below $\sim$4000 km s^{-1}, and we do not have data above $\sim$12 050 km s^{-1}, between these limits their plotted values are mostly similar to ours. In their fig. 14, the Fe II λ5169 velocities are lower than that of the model for high velocities, and their ratio reaches 1 between 5000 and 4000 km s^{-1}, just like our data. The situation is somewhat different for Hβ. At high velocities the two results are consistent: above $\sim$11 000 km s^{-1}, the data by Dessart & Hillier (2005b), as well as ours, are around 1. However, their velocity ratio exceeds 1 at $\sim$8000 km s^{-1} and has a highest value of 1.15 for Hβ. It is much lower than our results in Fig. 7. In the case of SN 2004et, our velocity ratio goes as high as 2.5. It must be noted, however, that the model spectra used by Dessart & Hillier (2005b) were tailored to represent SNe 1987A and 1999em (D05). The latter object is also in our sample, and our $v_{\rm H\beta}$ to $v_{\rm model}$ ratio for that particular SN is similar to the results of Dessart & Hillier (2005b). Thus, it is probable that the lower $v_{\rm H\beta}/v_{\rm model}$ ratio of Dessart & Hillier (2005b) is due to the limited parameter range of their CMFGEN models used to create their plot.

Recently, Roy et al. (2011) published a study of velocity measurement for the Type II-P SN 2008gz. They applied a similar technique of using SYNOW to fit Fe II features around 5000 Å. They also estimated the velocity from the absorption minima of these lines. They obtained 4200 ± 400 km s^{-1} and 4000 ± 300 km s^{-1} for $v_{\rm model}$ and $v_{\rm Fe}$, respectively, from a +87-d spectrum. This result is consistent with our findings plotted in Fig. 7: $v_{\rm Fe}$ is practically equal to $v_{\rm model}$ around 4000 km s^{-1}.

5.1 Velocity–velocity relations

Using the synthetic spectra of E96 and D05, Jones et al. (2009) also examined the relation between $v_{\rm H\beta}$ and $v_{\rm model}$. They found that their ratio can be described as

$$\frac{v_{\rm H\beta}}{v_{\rm model}} = \sum_{j=0}^{2} a_j v_{\rm H\beta}^j, \qquad (1)$$

where the values of a_j are given in Table 2. In Fig. 8(a) we plotted our data together with these polynomials. The polynomials based on the D05 models overestimate our $v_{\rm model}$ values (rms $\sigma = 0.412$),

Table 2. Polynomial coefficients for the $v_{\rm H\beta}$ and $v_{\rm Fe}$ to $v_{\rm model}$ ratio (equation 1).

j	0	1	2	σ	References
a_j (Hβ) (E96)	1.775	−1.435e–4	6.523e–9	0.30	1
a_j (Hβ) (D05)	1.014	4.764e–6	−7.015e–10	0.41	1
a_j (Hβ)	1.528	−1.551e–5	−3.462e–9	0.27	2
a_j (Hβ) without 04et	1.578	−8.573e–5	3.017e–9	0.17	2
a_j (Fe II λ5169)	1.641	−2.297e–4	1.751e–8	0.11	2

References. (1) Jones et al. (2009); (2) this paper.

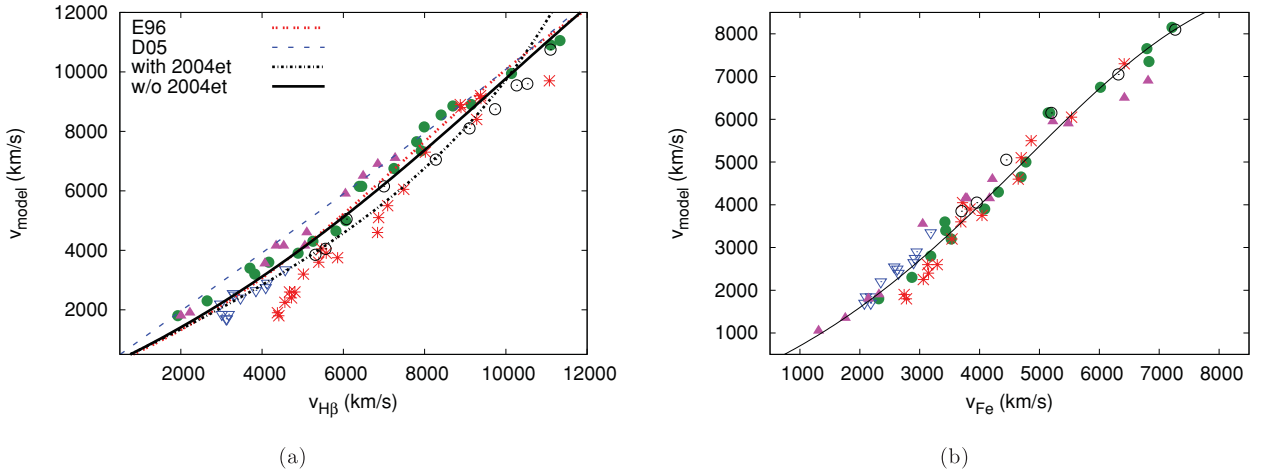

(a) (b)

Figure 8. (a) The plot of $v_{\rm model}$ against $v_{\rm H\beta}$. The lines represent the polynomials calculated by Jones et al. (2009) (see text) based on the models of E96 (red dotted line) and D05 (blue dashed line). The result from our fitting on all SNe is plotted as a black dotted line while the fitting that omits SN 2004et is shown by a black solid line. (b) The same fitting as (a) but for $v_{\rm Fe}$ using all SNe. The symbols have the same meaning as in Fig. 4. The polynomial coefficients are given in Table 2.

while those from the E96 models provide a much better fit for all SNe except SN 2004et (rms $\sigma = 0.301$, but $\sigma = 0.178$ without the data of SN 2004et).

We fitted equation (1) to our data (Fig. 8a, black curve). The resulting a_j coefficients are given in Table 2. Our fit resulted in a much lower rms scatter, $\sigma = 0.276$. Repeating the fitting while omitting the data of SN 2004et, the result became very similar to that from the E96 models.

Since $v_{\rm Fe}$ is thought to be a better representative of the velocity at the photosphere than $v_{\rm H\beta}$, it is expected that $v_{\rm model}$ can be predicted with better accuracy by measuring $v_{\rm Fe}$. Indeed, Fig. 7 suggests that the $v_{\rm Fe}/v_{\rm model}$ ratio is almost the same from SN to SN, unlike the $v_{\rm H\beta}/v_{\rm model}$ ratio that can be quite different for different SNe. Thus, we repeated the fitting of equation (1) using $v_{\rm Fe}$ instead of $v_{\rm H\beta}$ (Fig. 8b). We found the rms scatter of $\sigma = 0.111$, which is much lower than that in the previous cases. The a_j coefficients of this fitting are also included in Table 2.

The tight relation between $v_{\rm Fe}$ and $v_{\rm model}$ in Fig. 8(b) suggests a possibility to *estimate* $v_{\rm model}$ from the measured $v_{\rm Fe}$ values. However, it is emphasized that SN-specific differences in the expansion velocities may exist; thus, model building for a particular SN, whenever possible, should always be preferred.

Nugent et al. (2006) found that $v_{\rm Fe}$ evolves as

$$v_{\rm Fe}(t)/v_{\rm Fe}(50\,{\rm d}) = ({\rm t}/50)^{\rm c}, \qquad (2)$$

where $c = -0.464 \pm 0.017$. After repeating the fitting of equation (2) to our data, we found the exponent to be $c = -0.663 \pm 0.01$. Then, since the data of SN 2005cs are very different from the rest of the sample, we omitted the velocities of SN 2005cs and repeated the fitting. This resulted in $c = -0.546 \pm 0.01$ (Fig. 9a). These two exponents marginally differ (at $\sim 1\sigma$) from the value given by Nugent et al. (2006). A possible source of this difference (besides the different velocity measurement techniques applied) may be that our sample covers the phases between +13 and +104 d, while the data by Nugent et al. (2006) are between +9 and +75 d.

We also examined how the SYNOW model velocities evolve in time. Combining equations (1) and (2), the following relation has

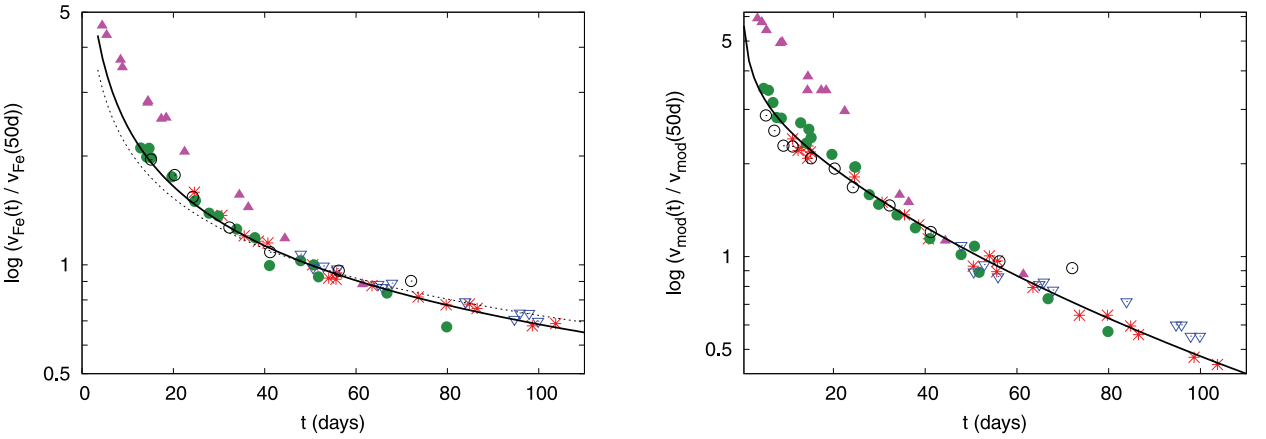

(a) (b)

Figure 9. The evolution of (a) $v_{\rm Fe}(t)/v_{\rm Fe}(50\,{\rm d})$ and (b) $v_{\rm model}(t)/v_{\rm model}(50\,{\rm d})$. The dashed line shows the result of Nugent et al. (2006), while the solid lines are from our fittings (see text). The data of SN 2005cs (filled triangles) were excluded from the fitting. The symbols have the same meaning as in Fig. 4.

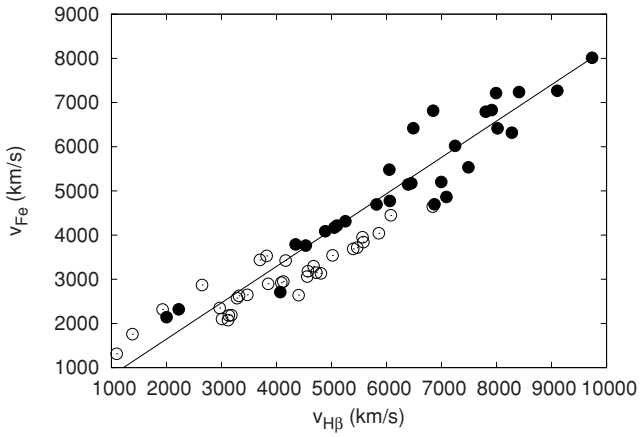

Figure 10. The relation between the measured $v_{\rm Fe}$ and $v_{\rm H\beta}$ values. The empty circles show the data taken after day 40, while the filled circles refer to data taken before day 40. The line shows the fit to the filled circles only.

been derived (again, excluding SN 2005cs from the sample):

$$v_{\rm model}(t)/v_{\rm model}(50\,{\rm d}) = \frac{({\rm t}/50)^{-0.210\pm0.11}}{\sum_{\rm j=0}^{2} {\rm b_j}({\rm t}/50)^{\rm j}}, \quad (3)$$

where $b_0 = 0.467 \pm 0.15$, $b_1 = 0.327 \pm 0.23$ and $b_2 = 0.174 \pm 0.11$. The rms scatter is $\sigma = 0.148$ (Fig. 9b).

As mentioned in Section 3.1, using SDSS data Poznanski et al. (2010) examined the correlation between velocities measured from the absorption minima of Hβ and Fe II λ5169 lines (see Fig. 10). They found that there is a linear relation given by $v_{\rm Fe}(50{\rm d}) = a\, v_{\rm H\beta}(50\,{\rm d})$, where $a = 0.84 \pm 0.05$. Using our sample, we repeated their fitting. First, we used all epochs where both $v_{\rm H\beta}$ and $v_{\rm Fe}$ were measured. The slope of the fitted line was $a = 0.791 \pm 0.012$ ($\sigma = 0.146$). Then, we kept only the velocities obtained before day 40 (similar to Poznanski et al. 2010). This resulted in $a = 0.823 \pm 0.015$ ($\sigma = 0.102$), which is basically the same as found by Poznanski et al. (2010). Thus, our study fully confirms the results of Poznanski et al. (2010), but extends the validity of the relation towards later phases.

6 IMPLICATIONS FOR DISTANCE MEASUREMENTS

Improving the accuracy of the velocity measurements has an important aspect in measuring extragalactic distances with SCM or EPM (cf. Section 1). Both SCM and EPM need velocities; thus, the results of this paper can be significant for both techniques.

SCM was calibrated using $v_{\rm Fe}$ on day +50. However, in many cases, getting a spectrum at or around day +50 is not possible. In these cases, equation (2) can be used to estimate $v_{\rm Fe}(50\,{\rm d})$. We have improved the exponent in equation (2) as -0.546 ± 0.01, based on more data obtained on a wider range of phases than previously. The difference between our result and the previous curve (Nugent et al. 2006) is the highest around day +20 (Fig. 9). The new curve may result in better constrained $v_{\rm Fe}(50\,{\rm d})$ when only early-phase spectra obtained around day +20 are available.

However, there are several drawbacks of SCM. For example, the uncertainty in the moment of explosion, i.e. in determining the phase of a particular spectrum, can lead to a significant error in the distance determination. Moreover, as the example of SN 2005cs shows in Fig. 9, some Type II-P SNe can deviate significantly from the average, especially during early phases. Thus, one should be careful when such an interpolation or extrapolation is to be applied. The example of SN 2005cs suggests that multi-epoch spectroscopic observations should always be preferred against single-epoch spectra when distance determination is the aim.

Table 3. EPM distances of the five SNe using different velocities.

SN	D (Mpc)		Photometry[a]
	With $v_{\rm model}$	With $v_{\rm Fe}$	
1999em	12.5 (1.4)	9.7 (0.8)	1, 2, 3
2004dj	3.6 (0.6)	3.7 (0.8)	4, 5
2004et	4.8 (0.4)	4.8 (0.6)	6, 7
2005cs	8.6 (0.2)	7.5 (0.2)	8
2006bp	20.7 (1.8)	18.6 (1.5)	9

[a]Sources of photometry: (1) Hamuy et al. (2001); (2) Leonard et al. (2002); (3) Elmhamdi et al. (2003); (4) Vinkó et al. (2006); (5) Tsvetkov et al. (2008); (6) Maguire et al. (2010b); (7) Sahu et al. (2006); (8) Pastorello et al. (2009); (9) Dessart et al. (2008).

The case of EPM is different. Since this method does not require calibration, but needs multi-epoch data, deviations in the measured velocities have a higher impact. To show this, we calculated the EPM distances of all five SNe via the method described in Vinkó & Takáts (2007). We used two sets of velocities for each SNe: (i) from the absorption minimum of the Fe II λ5169 line and (ii) $v_{\rm model}$ determined in Section 3.4.

The resulted distances are given in Table 3. The correction factors of D05 were applied for all SNe. Usually the photometric data were interpolated to the epochs of the velocities. However, for SN 2004dj, equations (2) and (3) were used to extrapolate the velocity data to the photometric epochs, because of the low number of spectra taken before day +50, i.e. during the expansion of the photosphere.

6.1 SN 1999em

Data on SN 1999em in NGC 1637 were used for distance determination with EPM several times. Hamuy et al. (2001) used cross-correlation velocities (with the model spectra of E96 as the template set) and the correction factors of E96 to obtain the distance of 7.8 ± 0.5 Mpc. Using absorption minimum velocities and the same correction factors, Leonard et al. (2002) determined the distance as 8.2 ± 0.6 Mpc, while Elmhamdi et al. (2003) obtained 7.8 ± 0.3 Mpc. On the other hand, Leonard et al. (2003) determined the distance of NGC 1637 using Cepheids as 11.7 ± 1 Mpc, which is significantly higher. Using the SEAM method, Baron et al. (2004) got 12.5 ± 1.8 Mpc. With the velocities of their CMFGEN models and the correction factors of D05, Dessart & Hillier (2006) derived 11.5 ± 1 Mpc, and with an approach similar to that of Baron et al. (2004), they obtained 12.2 ± 2 Mpc. Recently, Jones et al. (2009) estimated the photospheric velocity from $v_{\rm H\beta}$ (equation 1), and derived 9.3 ± 0.5 and 13.9 ± 1.4 Mpc by using the correction factors of E96 and D05, respectively.

We have repeated the EPM analysis using D05 correction factors and our $v_{\rm model}$ velocities. This resulted in 12.5 ± 1.4 Mpc, which is in good agreement with the Cepheid and SEAM distances and that of Dessart & Hillier (2006) using the velocities determined from their CMFGEN models. Instead, applying the $v_{\rm Fe}$ velocities (extrapolating for the first few points using equation 2), the distance decreased to 9.7 ± 0.8 Mpc. The disagreement between these two distances is roughly the same as that due to the application of different correction factors (see above). The distance obtained from adopting the

$v_{\rm model}$ velocities is in much better agreement with the independent Cepheid-based distance to the host galaxy. It suggests that the application of the proper velocity data is important for obtaining more realistic and bias-free distances from Type II-P SNe.

6.2 SN 2004dj

There are many published distances for the host galaxy of SN 2004dj (NGC 2403), but they show a large scatter, being between 2.88 and 6.43 Mpc, according to the NASA/IPAC Extragalactic Database (NED)[3].

In the case of this SN, the velocity curve was extrapolated using equations (2) and (3) to the epochs of the photometry of Vinkó et al. (2006) and Tsvetkov, Goranskij & Pavlyuk (2008). The distances from the two velocity curves agree very well ($D = 3.6 \pm 0.6$ and 3.7 ± 0.8 Mpc, respectively; Table 3) and they are also in very good agreement with the result of Vinkó et al. (2006).

6.3 SN 2004et

Similarly, the distances of NGC 6946, the host galaxy of SN 2004et, show a large scatter in the range of 4.7–7.2 Mpc (NED). $D \sim 4.7$ Mpc was derived recently by Poznanski et al. (2009) using SCM.

Our result supports this shorter value. The EPM analysis with both $v_{\rm model}$ and $v_{\rm Fe}$ (after extrapolation to the early phases by equation 2) gave 4.8 Mpc (Table 3).

6.4 SN 2005cs

In the case of SN 2005cs, the application of $v_{\rm model}$ resulted in a considerably longer distance (8.6 ± 0.2 Mpc) than that using $v_{\rm Fe}$ (7.5 ± 0.2 Mpc). This longer distance is in good agreement with a recent study by Vinkó et al. (2011), who determined the distance of M51 via EPM by combining the data of SNe 2011dh and 2005cs, and obtained 8.4 ± 0.7 Mpc. The reason for the slight difference between their result and ours with $v_{\rm model}$ (although both papers used the same photometry, velocities and method) is that, unlike Vinkó et al. (2011), we did not fix the moment of explosion in EPM. Instead, we also optimized that parameter to keep consistency with the analysis of all the other objects in this paper.

6.5 SN 2006bp

For SN 2006bp and its host galaxy, NGC 3953, the distances are between 15.7 and 21.0 Mpc (NED). Both of our results fit into this wide range, but with the usage of $v_{\rm model}$ we obtained slightly longer values (20.7 ± 1.8 Mpc) than with $v_{\rm Fe}$ (18.6 ± 1.5 Mpc), the latter being closer to the distance of Dessart et al. (2008), i.e. 17.1 and 17.5 Mpc from SEAM and SCM, respectively.

7 CONCLUSIONS

In this paper we investigated three methods for estimating photospheric velocities of Type II-P SNe. We focused on building model spectra with SYNOW and compared the resulting $v_{\rm model}$ velocities with those obtained by cross-correlation or simply measuring absorption minima of P Cygni features. Based on a sample of 81 spectra from five SNe, we showed that SYNOW provides photospheric velocities very similar to those derived by more sophisticated modelling codes, but in a faster, less computation-intensive way. This approach may be more extensively applicable, yet it preserves the advantages of using physically consistent model spectra to estimate parameters of SNe non-interactively, and without relying mostly on eye-ball estimates and human decisions.

We illustrated that the cross-correlation- and absorption minimum velocities, i.e. those determined by more conventional methods, suffer from phase-dependent systematic deviations from the model velocities. This was already known from previous studies (e.g. Dessart & Hillier 2005b), but we have extended the phase coverage of the modelled spectra and revealed that such deviations become stronger below $v_{\rm phot} \sim 3000$ km s^{-1}, i.e. after day +60. At these late phases, $v_{\rm Fe}$ may overestimate $v_{\rm model}$ by 30–50 per cent depending on the atmospheric properties of the particular SN.

Based on these results, we verified and updated the relations between the photospheric velocities and the ones estimated from the Doppler shifts of the absorption minima of individual spectral lines. It was found that while the $v_{\rm Fe}/v_{\rm model}$ ratio appears to be nearly the same for all SNe studied here, it is not true for the velocities from the Hβ line. We have derived a power-law relation to estimate $v_{\rm model}$ from $v_{\rm Fe}$ and/or $v_{\rm H\beta}$, but due to the possibility of SN-dependent systematic deviations, we recommend the computation of parametrized models, whenever possible.

Using the model velocities, we re-determined the distances of the five SNe via EPM, and compared them with the ones calculated by using $v_{\rm Fe}$. The distances obtained from $v_{\rm model}$ are similar or slightly higher than those obtained with $v_{\rm Fe}$. For SN 1999em, which is the most thoroughly studied object in our sample, we were able to show that by using the model velocities, the derived distance is more consistent with the Cepheid-based distance to the host galaxy. Although such a comparison was not possible for the other SNe due to the lack of reliable Cepheid distances, this result underlines the importance of the velocity measurement method in SN distance studies.

Despite its numerous advantages, EPM also suffers from caveats. One of them is the need for many photometric data and contemporaneous velocities (i.e. spectra) covering most of the plateau phase. This is hardly achievable for most SNe. A possible solution may be a careful interpolation between the measured data points. Previously, the weakest link was the poorly resolved velocity curve; thus, mainly the light curves were interpolated to the moments of velocity measurements (e.g. Hamuy 2002). Based on our results in Section 4, the interpolation of the velocity curve to the epochs of photometric data via equation (3) may also be a possibility, resulting in a better sampled data set for EPM. We intend to demonstrate the application of this approach for new SNe in a future paper (Takáts et al., in preparation).

ACKNOWLEDGMENTS

This project is supported by the European Union and co-funded by the European Social Fund through the TÁMOP 4.2.2/B-10/1-2010-0012 grant. This work has also been partly supported by the Hungarian OTKA grant K76816, the Hungarian National Office of Research and Technology, NSF grant AST-0707769 and the Texas Advanced Research Project grant ARP-0094 for J. C. Wheeler at University of Texas at Austin. We thank Dr A. Pastorello and Dr K. Maguire for providing spectra of SNe 2005cs and 2004et in digital form, and Dr L. Dessart for providing CMFGEN models used in this paper. We are grateful to Prof S. Rucinski, S. Mochnacki, T. Bolton and R. Garrison (University of Toronto) for generously offering their telescope time used for observing SN 2004et at DDO in 2004. We also thank the referee, Dr D. Poznanski, for his thorough report that helped us to improve the manuscript. This research has made use of NASA's Astrophysics Data system, the Supernova

[3] Available from http://ned.ipac.caltech.edu/

Spectrum Archive (SUSPECT) hosted by University of Oklahoma, and the NASA/IPAC Extragalactic Database (NED) which is operated by the Jet Propulsion Laboratory, California Institute of Technology, under contract with the National Aeronautics and Space Administration.

REFERENCES

Baron E., Nugent P. E., Branch D., Hauschildt P. H., 2004, ApJ, 616, L91
Blondin S., Tonry J. L., 2007, ApJ, 666, 1024
Branch D. et al., 2002, ApJ, 566, 1005
Chugai N. N., Fabrika S. N., Sholukhova O. N., Goranskij V. P., Abolmasov P. K., Vlasyuk V. V., 2005, Astron. Lett., 31, 792
Crockett R. M., Smartt S. J., Pastorello A., Eldridge J. J., Stephens A. W., Maund J. R., Mattila S., 2011, MNRAS, 410, 2767
D'Andrea C. B. et al., 2010, ApJ, 708, 661
Dessart L., Hillier D. J., 2005a, A&A, 437, 667 (D05)
Dessart L., Hillier D. J., 2005b, A&A, 439, 671
Dessart L., Hillier D. J., 2006, A&A, 447, 691
Dessart L. et al., 2008, ApJ, 675, 644
Eastman R. G., Schmidt B. P., Kirshner R., 1996, ApJ, 466, 911 (E96)
Eldridge J. J., Mattila S., Smartt S. J., 2007, MNRAS, 376, L52
Elmhamdi A. et al., 2003, MNRAS, 338, 939
Fisher A., 1999, PhD thesis, Univ. Oklahoma
Gaskell C. M., Cappellaro E., Dinerstein H. L., Garnett D. R., Harkness R. P., Wheeler J. C., 1986, ApJ, 306, L77
Hamuy M., 2002, PhD thesis, Univ. Arizona
Hamuy M., 2003, in Marcaide J.-M., Weiler K. W., eds, Proc. IAU Colloq. 192, Cosmic Explosions: On the 10th Anniversary of SN 1993J. Springer, Berlin, p. 535
Hamuy M., Pinto P. A., 2002, ApJ, 566, L63
Hamuy M. et al., 2001, ApJ, 558, 615
Hatano K., Branch D., Fisher A., Millard J., Baron E., 1999, ApJS, 121, 233
Immler S. et al., 2007, ApJ, 664, 435
Jones M. I. et al., 2009, ApJ, 696, 1176
Kasen D., Branch D., Baron E., Jeffery D., 2002, ApJ, 565, 380
Kirshner R. P., Kwan J., 1974, ApJ, 193, 27
Kloehr W., Muendlein R., Li W., Yamaoka H., Itagaki K., 2005, IAU Circ., 8553, 1
Kotak R., Meikle P., van Dyk S. D., Höflich P. A., Mattila S., 2005, ApJ, 628, L123
Leonard D. C. et al., 2002, PASP, 114, 35
Leonard D. C., Kanbur S. M., Ngeow C. C., Tanvir N. R., 2003, ApJ, 594, L247
Li W. D., 1999, IAU Circ., 7294, 1
Li W., Van Dyk S. D., Filippenko A. V., Cuillandre J.-C., 2005, PASP, 117, 121
Maguire K., Kotak R., Smartt S. J., Pastorello A., Hamuy M., Bufano F., 2010a, MNRAS, 403, L11
Maguire K. et al., 2010b, MNRAS, 404, 981
Maíz-Apellániz J., Bond H. E., Siegel M. H., Lipkin Y., Maoz D., Ofek E. O., Poznanski D., 2004, ApJ, 615, L113
Maund J. R., Smartt S. J., Danziger I. J., 2005, MNRAS, 364, L33
Misra K., Pooley D., Chandra P., Bhattacharya D., Ray A. K., Sagar R., Lewin W. H. G., 2007, MNRAS, 381, 280
Nakano S., Itagaki K., 2006, IAU Circ., 8700, 4
Nakano S., Itagaki K., Bouma R. J., Lehky M., Hornoch K., 2004, IAU Circ., 8377, 1
Nugent P. et al., 2006, ApJ, 645, 841
Pastorello A. et al., 2006, MNRAS, 370, 1752
Pastorello A. et al., 2009, MNRAS, 394, 2266
Poznanski D. et al., 2009, ApJ, 694, 1067
Poznanski D., Nugent P. E., Filippenko A. V., 2010, ApJ, 721, 956
Quimby R. M., Wheeler J. C., Höflich P., Akerlof C. W., Brown P. J., Rykoff E. S., 2007, ApJ, 666, 1093
Roy R. et al., 2011, MNRAS, 414, 167
Sahu D. K., Anupama G. C., Srividya S., Muneer S., 2006, MNRAS, 372, 1315
Smartt S. J., 2009, ARA&A, 47, 63
Smartt S. J., Gilmore G. F., Tout C. A., Hodgkin S. T., 2002, ApJ, 565, 1089
Smartt S. J., Eldridge J. J., Crockett R. M., Maund J. R., 2009, MNRAS, 395, 1409
Takáts K., Vinkó J., 2006, MNRAS, 372, 1735
Thomas R. C., Nugent P. E., Meza J. C., 2011, PASP, 123, 237
Tsvetkov D. Y., Goranskij V., Pavlyuk N., 2008, Perem. Zvezdy, 28, 8
Utrobin V. P., 2007, A&A, 461, 233
Utrobin V. P., Chugai N. N., 2008, A&A, 491, 507
Utrobin V. P., Chugai N. N., 2009, A&A, 506, 829
Vinkó J., Takáts K., 2007, in Immler S., Weiler K., McCray R., eds, AIP Conf. Proc. Vol. 937, Supernova 1987A: 20 Years After. Am. Inst. Phys., Melville, p. 394
Vinkó J. et al., 2006, MNRAS, 369, 1780
Vinkó J. et al., 2009, ApJ, 695, 619
Vinkó J. et al., 2011, preprint (arXiv:1111.0596)
Wang X., Yang Y., Zhang T., Ma J., Zhou X., Li W., Lou Y.-Q., Li Z., 2005, ApJ, 626, L89
Zhang T., Wang X., Li W., Zhou X., Ma J., Jiang Z., Chen J., 2006, AJ, 131, 2245
Zwitter T., Munari U., Moretti S., 2004, IAU Circ., 8413, 1

APPENDIX A: EARLY SPECTRA OF SN 2004et

Soon after its discovery (Zwitter et al. 2004), six low-resolution optical spectra of SN 2004et were taken at the David Dunlap Observatory, Canada, with the Cassegrain spectrograph mounted on the 74-inch telescope. The spectra covered the 4000–8000 Å regime with a resolution of ∼800 at 6000 Å (see the details on the data reduction in Vinkó et al. 2006). Due to the fixed north–south slit direction, the spectra could not be taken at the parallactic angle; thus, the slope of the continuum in the blue is affected by differential refraction. Table A1 contains the journal of these observations and the spectra are plotted in Fig. A1.

Table A1. Journal of spectroscopic observations of SN 2004et.

Date	JD 245 0000	Phase (d)	Airmass	Observer[a]
2004-10-03	3281.6	+11	1.2	JT, TK
2004-10-04	3282.8	+12	2.0	SM, JT
2004-10-05	3283.5	+13	1.1	HD, TK
2004-10-06	3284.9	+14	2.3	HD, JT
2004-10-07	3285.5	+15	1.1	HD, JT
2004-10-08	3286.9	+16	1.7	JT, JG

[a] *Observers*. JT, J. Thomson; TK, T. Koktay; SM, S. Mochnacki; HD, H. DeBond; JG, J. Grunhut.

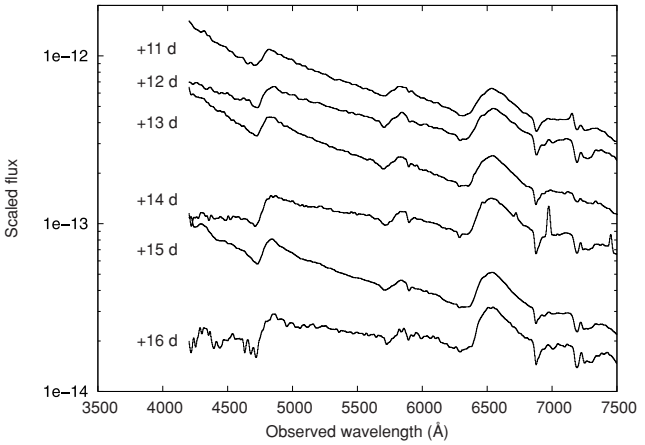

Figure A1. Early spectra of SN 2004et.

Table B1. The velocities (in km s^{-1}) obtained with different techniques: the photospheric velocities from the best-fitting SYNOW models ($v_{\rm model}$), the Doppler shift of the absorption minima of Hβ and Fe II λ5169 features ($v_{\rm H\beta}$ and $v_{\rm Fe}$, respectively) and the cross-correlation velocities from templates consisting of the observed spectra of SN 1999em ($v_{\rm cc\#1}$) and the CMFGEN models ($v_{\rm cc\#2}$). The phase (in days) was calculated relative to the date in Table 1.

SN 1999em						SN 2004et					
Phase	$v_{\rm model}$	$v_{\rm H\beta}$	$v_{\rm Fe}$	$v_{\rm cc\#1}$	$v_{\rm cc\#2}$	Phase	$v_{\rm model}$	$v_{\rm H\beta}$	$v_{\rm Fe}$	$v_{\rm cc\#1}$	$v_{\rm cc\#2}$
4.79	11 050 (300)	11 332	–		10341 (454)	11.10	9700 (450)	11072	–	9951 (153)	8781 (1316)
5.84	10 900 (350)	11 101	–		9858 (888)	12.30	8900 (250)	8878	–	8605 (86)	8470 (681)
6.84	9950 (250)	10 141	–		9112 (878)	13.00	9100 (400)	9386	–	9724 (117)	8786 (1099)
7.64	8900 (200)	9148	–		8383 (832)	14.40	9200 (400)	9375	–	7617 (71)	8570 (482)
8.67	8850 (150)	8697	–		8544 (491)	15.00	8800 (100)	8894	–	8635 (64)	8545 (524)
12.84	8550 (500)	8406	7236		8513 (497)	16.40	8400 (400)	9282	–	9110 (73)	9060 (545)
14.14	7350 (500)	7913	6829		7575 (289)	24.60	7300 (550)	8018	6416	6624 (49)	–
					...						

Table C1. The SYNOW parameters of the best-fitting models. The phases were calculated from the assumed moments of explosions listed in Table 1.

SN 1999em															
Phase	JD 245 1000	$\tau_{\rm ref}$											n	$T_{\rm bb}$	$v_{\rm phot}$
(d)	(d)	H I	He I	Na I	Si I	Si II	Ca II	Sc II	Ti II	Fe II	Ba II			(kK)	(km s^{-1})
4.79[a]	481.79	2.80	0.25										3.0	14.2	11 050
5.84[b]	482.84	3.50	0.20										3.0	12.0	10 900
6.84[b]	483.84	4.90	0.40										3.0	11.0	9950
7.64[a]	484.64	6.30	0.35										3.0	9.5	8900
8.67[a]	485.67	7.30	0.20										3.5	13.6	8850
12.84[b]	489.84	15.80	0.10										5.5	10.0	8550
14.14[b]	491.14	21.10		0.20						0.30			5.0	11.0	7350
							...								

APPENDIX B: SNe velocities measured with different techniques

In Table B1 we present the velocities obtained with SYNOW ($v_{\rm model}$; see Section 3.4), along with those measured from the absorption minima of Hβ and Fe II λ5169 ($v_{\rm H\beta}$ and $v_{\rm Fe}$), as well as those obtained with the cross-correlation method using the observed spectra of SN 1999em as templates ($v_{\rm cc\#1}$) and the CMFGEN models ($v_{\rm cc\#2}$).

APPENDIX C: PARAMETERS OF THE BEST-FITTING SYNOW MODELS

In Table C1 we present the parameters of the best-fitting SYNOW models, including $\tau_{\rm ref}$ of the main atoms/ions, the power-law exponent of the optical depth function (n), the photospheric temperature ($T_{\rm bb}$) and the photospheric velocity ($v_{\rm phot}$) (see Section 3.4 for details).

SUPPORTING INFORMATION

Additional Supporting Information may be found in the online version of this article:

Table B1. The velocities (in km s^{-1}) obtained with different techniques.
Table C1. The SYNOW parameters of the best-fitting models.

Please note: Wiley-Blackwell are not responsible for the content or functionality of any supporting materials supplied by the authors. Any queries (other than missing material) should be directed to the corresponding author for the article.

This paper has been typeset from a TEX/LATEX file prepared by the author.